

## Characterizing COTS IMU Performance in High Vacuum

Katherine Fowee, Dhruv Mathur, Noah Franks, Alina Alexeenko

Purdue University School of Aeronautics and Astronautics

701 W. Stadium Avenue West Lafayette, IN 47907; (765) 496-1864

kfowee@purdue.edu

### ABSTRACT

Using CubeSat/nanosat missions as technology demonstrators requires minimizing sources of potential failures from standard spacecraft bus components. Attitude determination and control is a critical component of most nanosat architectures, with angular rates and pointing of the craft being essential to telecommunications and often for the payload instruments as well. The lack of compact star sensors forces a reliance on Inertial Measurement Units (IMUs) for attitude determination and control. This research evaluated the UM7-LT COTS IMU performance by testing in low and high vacuum (milli-Torr and micro-Torr pressure) conditions. This device was not rated by manufacturers for usage in space environment. The performances of the accelerometers, gyroscopes, and magnetometers are characterized in these conditions, evaluating parameters of bias due to thermal effects. Additionally, Raspberry Pi 0W temperature data is evaluated in low and high vacuum. The analysis of thermal data at different vacuum levels using simple lumped capacitance method, allows to estimate the effective heat transfer coefficient and design the on-orbit duty-cycle to avoid overheating.

### INTRODUCTION

The space industry has been following the same miniaturization tendencies as the personal electronic, computer, and automation industries for more than three decades. With launch costs being associated with the mass and volume of a satellite, small satellites have become the platform of choice for academic and commercial breakout ventures.

The CubeSat Standard was originally developed by the California Polytechnic State University and Stanford University to develop an inexpensive, efficient, and straightforward platform for small payloads<sup>1,2</sup>. In the last 5 years, CubeSats have been a dominant platform, with over 700 launches since 2012, and 87% of small satellites launched in 2017 were CubeSats. In the same time period, approximately a quarter of small satellite launches have been academic with a majority of those being CubeSats<sup>3</sup>.

These trends highlight the utility of CubeSats as an educational platform, giving many students hands on experience in the design, manufacturing, and systems analysis required for developing any space mission architecture. While CubeSats are applicable to educational endeavors, they are a practical platform for technology development and national science investment, allowing an economic route for demonstration and testing of new space technologies<sup>4,5</sup>.

CubeSats fill a functional gap and allow for unique science objectives such as aerothermodynamic reentry chemistry or measuring the flux of solar-reflected energy leaving Earth in the upper atmosphere and permit the investigation of technologies to solve the unique challenges posed by space exploration<sup>6,7</sup>. Technology development accounts for approximately 90% of academic CubeSat launches and 7% of all commercial small satellite launches in the last 5 years<sup>3</sup>. In total, technology development missions and science missions comprise 12% and 26% of small satellite missions respectively<sup>8</sup>. NASA lists space technology development and maturation as a national investment to revolutionize space exploration and discovery and has recognized CubeSats as a valuable asset for this endeavor<sup>9,10</sup>.

As small satellites continue to be used for science experimentation and technology proof-of-concepts, it is more important than ever to ensure mission success for such projects. Due to size considerations, the usage of star trackers is precluded for Attitude Determination and Control Systems (ADCS) on CubeSats.

In addition to the basic function of the ADCS, many experiments or proofs of concept require attitude, orientation, and acceleration data to achieve full mission success. Technology development begins well

before a CubeSat mission and includes bench testing and testing in a relevant environment, such as vacuum or thermal vacuum chambers. As a sophisticated spacecraft bus is unnecessary for testing a single technology system on the ground, the ideal solution for such projects would be to use low-cost, commercial-off-the-shelf (COTS) components.

Instead of a bus, it is simpler to use a home robotics computer such as Raspberry Pi and Arduino with a component circuit board. These are readily available and have extensive documentation, but they are not rated for space flight. For position sensing, there are many COTS micro-electromechanical system (MEMS) inertial measurement units (IMU). An IMU is a sensor assembly that can provide acceleration and angular turning rate data<sup>11</sup>. This is typically accomplished through a combination of accelerometers, gyroscopes, and magnetometers aligned in a three-axis configuration. MEMS IMUs have micrometer to millimeter scale components that coexist on a single substrate<sup>12</sup>. Mass-produced MEMS sensors have similar reliability while being cheaper than their larger counterparts (Jansen). The gyroscopes are typically more useful to a satellite than the accelerometer as understanding the rotation characteristics is necessary

for station keeping and pointing. Accelerometers are able to provide data on aerodynamic drag or orbit change maneuvers.

Most COTS computers and IMUs are not intended for use in the space thermal and pressure environment and so are not tested for that environment. These devices do not always work well in low pressures as they struggle in the convection free environment. Table 1 includes a list of COTS IMUs flown or scheduled to fly on missions.

The objective of this research was to test a COTS IMU in low and high vacuum (milli-Torr to micro-Torr pressure) conditions, to characterize their thermal properties and behavior, as well as instrument behavior and suitability for usage in space, for CubeSat missions. This included testing hardware for the small and large vacuum chambers at the Aerospace Sciences Laboratory (ASL) at the Purdue University. The testing hardware would be able to test all 3 major functions of COTS IMUs, namely Accelerometer, Gyroscope and Magnetometer. As data were also collected on Raspberry Pis, this study was also used to assess their behavior in vacuum.

**Table 1 List of IMUs used for Small Satellite Missions**

Manufacturer	Model	Price	Flight Projects	Dimensions [mm]	Temperature [C]
Analog Devices	ADIS 16334 <sup>13</sup>	\$535.50	MicroMAS (MIT, USA, 2014) <sup>14</sup>		-20 to 70
Analog Devices	ADIS 16350 <sup>15</sup>		PurdueSat (Purdue, USA, 2009) <sup>16</sup>	23.5 x 23.0 x 23.5	-40 to 85
Analog Devices	ADIS 16405 <sup>17</sup>	\$625-729	SwampSat (Univ of Florida, USA, 2013) <sup>18</sup>	23.5 x 23.0 x 23.5	-40 to 85
Analog Devices	ADIS16365 <sup>19</sup>	\$633	Prox 1 (GeorgiaTech, USA, 2016) <sup>20</sup>	23.5 x 23.0 x 23.5	-40 to 85
Analog Devices	ADIS16485 <sup>21</sup>	\$1,697	QB-50 EntrySat (ISAE-Supaero, France, 2018) <sup>22</sup>	47 x 44 x 14	-40 to 85
Epson	M-G362 <sup>23</sup>		NASA iSAT (2018 scheduled, but delayed) <sup>24</sup>	24 x 24 x 10	-40 to 85
CH Robotics	UM7 <sup>25</sup>	\$140	ADE (Purdue, USA, 2018)	27 x 26 x 6.5	-40 to 85
VectorNav	VN-100 <sup>26</sup>	\$800	AeroCube-OCSD (NASA, 2015) <sup>27</sup>	24 x 22 x 3	-40 to 85
TDK Invensense	MPU 6050 <sup>28</sup>	\$8.29-40	LituaniaSat-1 (2014) <sup>29</sup>	4x4x0.9	-40 to 85
MicroStrain	LORD 3DM-GX5-10		ELaNa IV (Vermont Tech, 2013)	36.0 mm x 36.6 mm x 11.1 mm	-40 to 85

## TEST DEVICE OVERVIEW

### Inertial Measurement Unit – UM7-LT

The UM7-LT is an Micro-Electromechanical System (MEMS) Inertial Measurement Unit (IMU), which combines tri-axial data from accelerometer, rate gyro and magnetometer, using an Extended Kalman Filter (EKF) to produce attitude and orientation data<sup>25</sup>. The device is pictured in Figure 1.

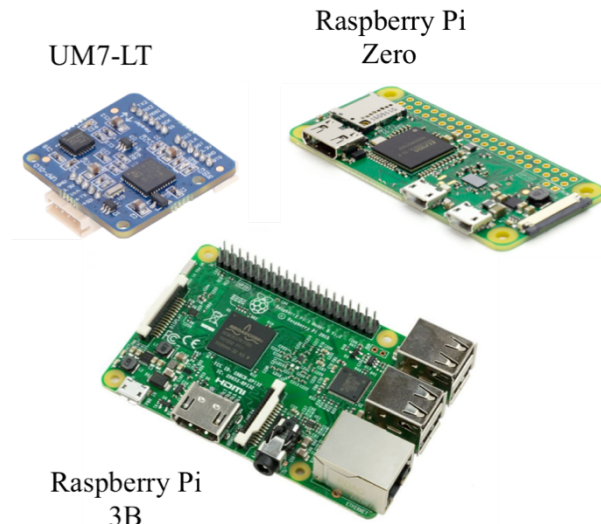


**Figure 1** UM7-LT, Raspberry Pi Zero, Raspberry Pi 3B

The UM7 is 27mm x 26mm x 6.5mm, and weighs 11 g. The IMU has an operating temperature range of -40 to +85 degrees Celsius. It operates at in the range of 4-5.5 V, drawing around 50mA at 5V<sup>25</sup>.

In our tests, we are utilizing the raw acceleration, gyro and magnetometer data, along with the temperature data as read by the UM7, to correct for thermal drift and bias and to calibrate the device to use in high vacuum conditions for attitude and acceleration control.

### Raspberry Pi Zero

The Raspberry Pi Zero (pictured in Figure 2) is 65mm x 31mm x 5mm. It has a single-core GHz Advanced Reduced Instruction Set Computing (RISC) Machine (ARM), 15MB of RAM, Bluetooth, and runs a MicroSD card. It is the smallest and cheapest computer available from Adafruit Industries. It is predominantly used in the hobbyist electronics industry, but is also a common bench-testing component<sup>33</sup>.

## TESTING AT ATMOSPHERIC PRESSURE CONDITIONS

Phase I of the test plan was formulated to achieve this - the in-air test under a FLIR Infrared camera would pinpoint the major heat source on the UM7 board, while the X-ray trace would show whether the heat-generating component could be disconnected, so as to ensure the IMU sensors would not experience temperature change.

The images from the FLIR IR camera (as seen in Figure 3) showed that the processing integrated circuit (IC) generated the majority of the heat, as opposed to the smaller MEMS sensor IC. The X-ray trace (shown in Figure 2) showed that the processing IC could not be removed from the board, as the connections between the output channel and the IMU sensor chip on the UM7 were connected with the processing IC in series. Since the heat source could not be removed, the next phase of testing was structured around testing the IMU in vacuum, establishing its operability in those conditions, and using the collected data to calibrate for thermal effects.

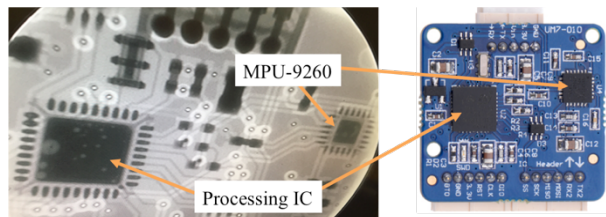


**Figure 2** The IMU under the X-Ray Camera

## TESTING AT LOW VACUUM PRESSURE CONDITIONS

The IMU was first tested in low vacuum pressure to determine the temperature range it would reach in absence of convective cooling by air. This was done to judge if the IMU would begin approaching its operational limit (85 degrees Celsius<sup>25</sup>). The low vacuum testing was completed in the small vacuum chamber. This is an airtight, 1 foot diameter by one foot tall acrylic cylinder evacuated by an Alcatel 2008A two-stage rotary vane pump that can pump down at 7 ft^3/min. The minimum pressure is 10 milli-Torr. Low vacuum tests of the UM7-LT were done in the 50-60 milli-Torr range. A Raspberry Pi 3B, kept outside of the chamber, was used to collect the data from the UM7-LT inside of the small vacuum chamber. In order to verify the value of the temperature reading from the UM7-LT,

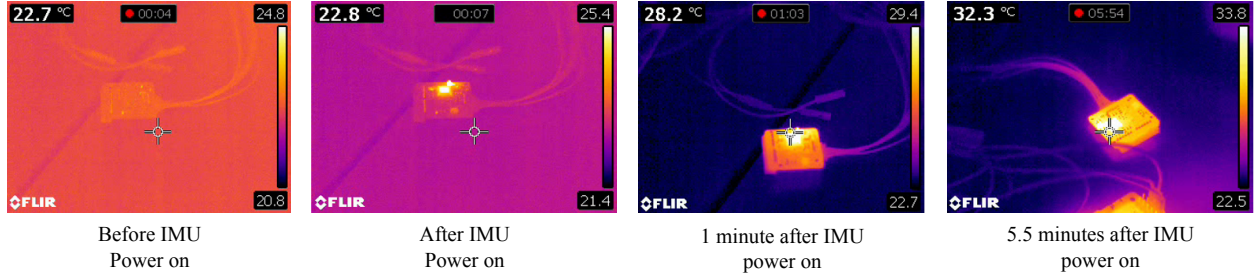


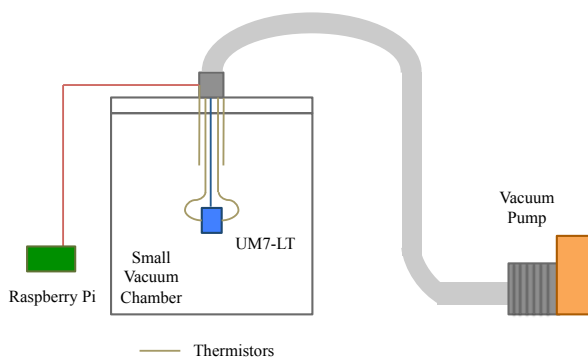
**Figure 3 FLIR Thermal Imaging on the UM7-LT**

two thermistors were placed on the processing IC (one on top of the IC and one on the bottom). As mentioned before, the processing unit was found to be the dominant heat generator on the IMU. Two thermistors were also measuring the ambient temperature within the small vacuum chamber. Figure 4 is a diagram of the test set up inside the small vacuum chamber. Table 2 lists the testing conditions for this test.

**Table 2 Low Vacuum Pressure Test Conditions**

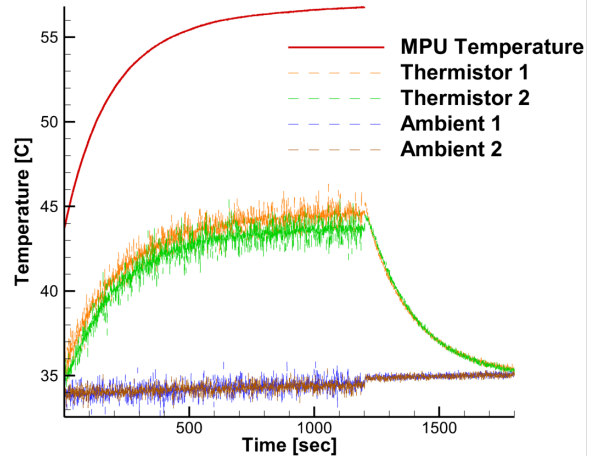
Initial Pressure	Initial Temperature	Final Temperature
52.2 milliTorr	43.8°C	56.7°C

Figure 5 shows the temperature profile of this test and the bias between the thermistor data and the IMU temperature data. The two thermistors on the processing IC followed the same profile as the IMU temperature sensor.



**Figure 4 Small Vacuum Chamber Testing Schematic**

The thermistors also tracked the cool down period after the IMU was completely powered off. In the small chamber it takes approximately ten minutes for the IMU to return to the initial temperature. The ambient temperature reading remained constant at 32°C. Testing showed that the temperature change during static tests did have a measurable effect on the outputs of the IMU.



**Figure 5 Temperature Profile of Low Vacuum Pressure Test**

When taking data in the thermal environment associated with low pressures, it will be necessary to offset or correct the error caused by heat accumulation in the sensor so as to properly understand the motion.

If the temperature of the sensor can affect the outputs from the gyroscope, accelerometer, and magnetometer enough, the computer could execute programs for stabilization that are unnecessary and possibly harmful.

Equations were fitted to the data with temperature as the independent variable. For each case polynomial fits with order 1 (equation 1) and 2 (equation 2) and an exponential fit (equation 3) was applied to the data. These fits are described by

$$v(T) = aT + b \quad (1)$$

$$v(T) = aT^2 + bT + c \quad (2)$$

$$v(T) = ae^{(bT)} \quad (3)$$

where  $v(T)$  is the expected value of the output based on the fit,  $a$ ,  $b$ , and  $c$  are coefficients, and  $T$  is temperature.

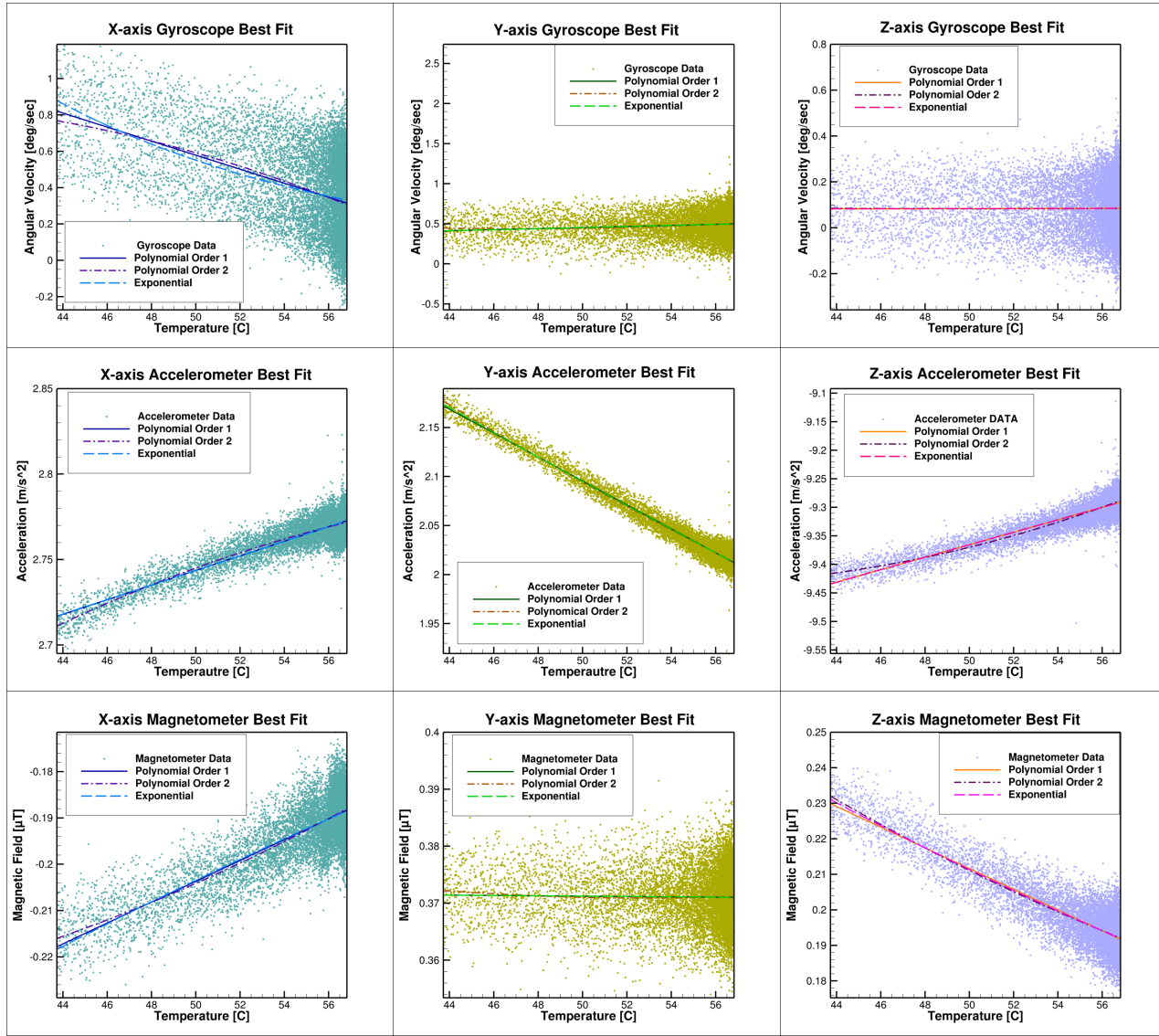


**Figure 6 Low Vacuum Pressure Raw Gyroscope, Accelerometer, and Magnetometer Data Against Temperature with Best Fit Approximations**

Figure 6 contains raw data from the gyroscopes, accelerometers, and magnetometers versus termperature with the fitted equations

Tables 3-5 list the  $r^2$  and root mean squared error (rmse) data for these three fits for each axis of the gyroscope, accelerometer, and magnetometer

The y-axis gyroscope, z-axis gyroscope, and y-axis magnetometer data do not vary with temperature. The x-axis and z-axis accelerometers and magnetometers increase as temperature increases while the x-axis gyroscope and y-axis accelerometer both decrease as temperature increases.

**Table 3 Gyroscope Best-Fit Line Statistical Data**

	x-axis	y-axis	z-axis
<b>1<sup>st</sup> order polynomial <math>r^2</math></b>	0.22	0.02	0.00
<b>1<sup>st</sup> order polynomial rmse</b>	0.22	0.16	0.12
<b>2<sup>nd</sup> order polynomial <math>r^2</math></b>	0.22	0.02	0.00
<b>2<sup>nd</sup> order polynomial rmse</b>	0.22	0.16	0.12
<b>Exponential <math>r^2</math></b>	0.21	0.02	0.00
<b>Exponential rmse</b>	0.22	0.16	0.12

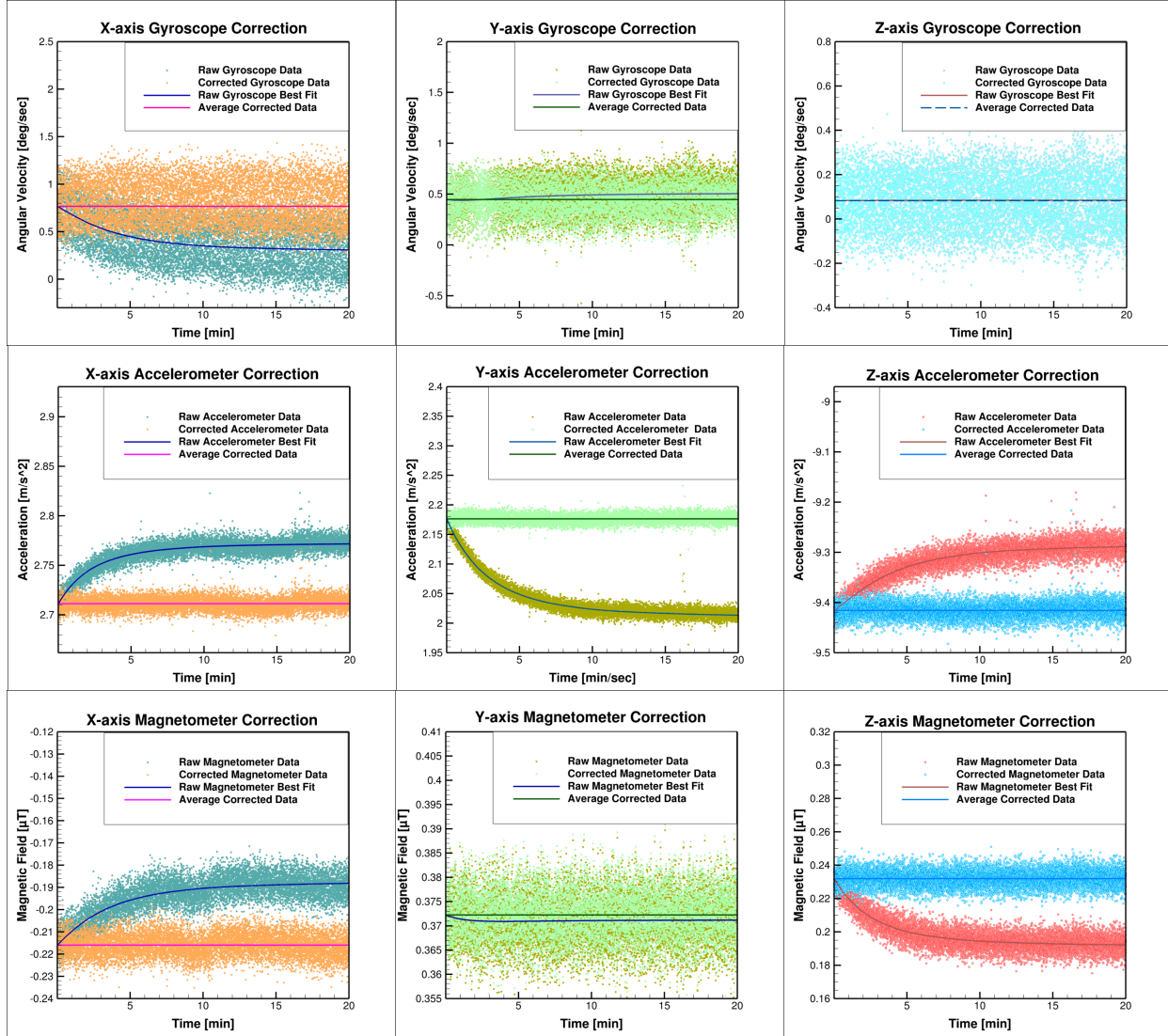


**Figure 7 Corrected Low Vacuum Gyroscope, Accelerometer, and Magnetometer Data**

**Table 4 Accelerometer Best-Fit Line Statistical Data**

	x-axis	y-axis	z-axis
1 <sup>st</sup> order polynomial r <sup>2</sup>	0.79	0.96	0.81
1 <sup>st</sup> order polynomial rmse	0.01	0.01	0.02
2 <sup>nd</sup> order polynomial r <sup>2</sup>	0.79	0.96	0.82
2 <sup>nd</sup> order polynomial rmse	0.01	0.01	0.02
Exponential r^2	0.79	0.96	0.81
Exponential rmse	0.01	0.01	0.02

Tables 3-5 also show that where a fit is best applicable, the second order polynomial fit is most appropriate as the  $r^2$  term is closest to one and the rmse is lowest. The value of these approximate equations relating temperature with the outputs from the gyroscope, accelerometer, and magnetometer is the users ability to correct for the drift experience in these outputs.

Figure 7 shows the raw data versus data that has been corrected for thermal drift by removing the drift (approximated with the best fit equations) from the raw data. The relationship:

$$w(t) = u(t) - v(t) + u_0 \quad (4)$$

where  $u$  is the sensor output value at time  $t$ ,  $v$  is the value of the fit at the temperature corresponding to the time  $t$ , and  $u_0$  is the initial value of the sensor output.

On each graph, the second order polynomial fit has been plotted over the raw data. The corrected data now implies that the UM7 is static and unmoving.

**Table 5 Magnetometer Best-Fit Line Statistical Data**

	x-axis	y-axis	z-axis
1 <sup>st</sup> order polynomial r <sup>2</sup>	0.64	0.00	0.75
1 <sup>st</sup> order polynomial rmse	0.01	0.01	0.01
2 <sup>nd</sup> order polynomial r <sup>2</sup>	0.64	0.00	0.75
2 <sup>nd</sup> order polynomial rmse	0.01	0.01	0.01
Exponential r^2	0.64	0.00	0.75
Exponential rmse	0.01	0.01	0.01

### TESTING AT HIGH VACUUM PRESSURE CONDITIONS

Having established that the IMU would not overheat in low vacuum, the next steps were to perform static tests in high vacuum, and using the collected data for calibration and correction for thermal effects. These tests were conducted in the pressure range of  $7.8 \times 10^{-6}$  -  $1.1 \times 10^{-5}$  Torr.

Tests over a larger temperature range would provide a more accurate approximation; a larger temperature range is not feasible given that the test covers the temperatures available with limited convection

Large vacuum testing was completed in the large vacuum chamber. The large vacuum chamber is 5 feet in diameter, 7 feet long, and made of cast aluminum. Two mechanical pumps, a two-stage positive displacement pump and a blower bring the chamber to medium vacuum (~1 milli-Torr) and the high-throughput Varian HS-20 diffusion pump brings the chamber to high vacuum (~1 micro-Torr). The chamber is shown in Figure 8

The test set up is shown in Figure 9. The UM7-LT was thermally isolated and resting on the static table inside of the vacuum chamber with the gravity vector aligned along the -Z axis of the accelerometer. Data is collected by a Raspberry Pi 3B, shown in Figure 9. The Pi has a conductive heat sink to dissipate heat.

The Raspberry Pi 3B is connected by Ethernet to a computer outside of the large vacuum chamber. There were 3 separate tests done inside of the large vacuum chamber: a 10-minute interval test, a staggered interval test, and a test with longer off intervals.

### 10-Minute Interval Test

There are many cases where certain sensors may be turned off during a mission to save power. The UM7-LT was cycled in the large vacuum chamber to simulate such activity. The 10-minute interval test consisted of three 10-minute measurement periods followed by 10 minutes of shutdown. Table 6 includes the test conditions for the 10-minute interval test. Figure 10 shows the temperature profile for the entire test, the comparison of each intervals change in temperature, and the behavior of the y-axis accelerometer during the intervals.

The plot shows that in the micro-Torr range, 10 minutes is not enough time to return to the initial temperature, despite 10 minutes being enough time to return to the initial temperature at the milli-Torr range. The individual interval curves vary only slightly when compared directly to each other, with the second and third curves being almost identical in profile. The total change over ten minutes varies by less than a degree, the starting temperature varies by 3 degrees, and the final temperature varies by approximately 1 degree. The y-axis accelerometer is shown as an example.



**Figure 8 Large Vacuum Chamber at the Aerospace Sciences Laboratory at Purdue University**

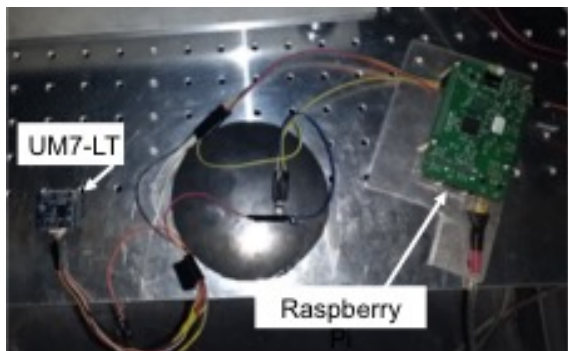


**Figure 9 Large Vacuum Chamber Static Test Set Up with UM7-LT and Raspberry Pi 3B**

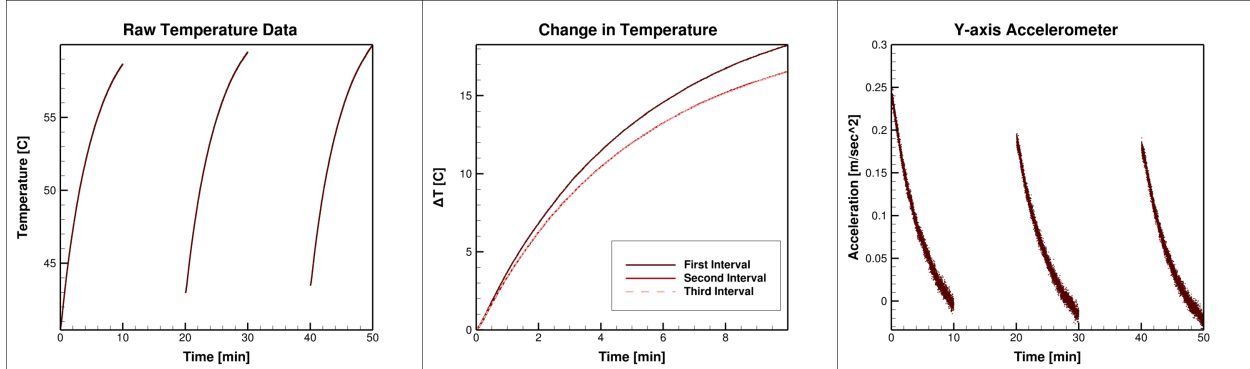


**Figure 10 10-Minute Interval Test at High Vacuum**

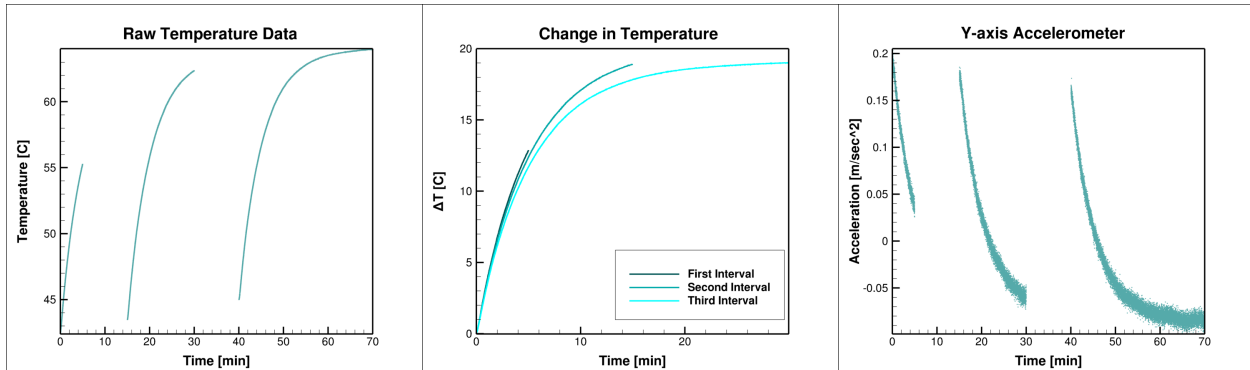


**Figure 11 Staggered Interval Test at High Vacuum**

Just as in the low vacuum test, many of the sensor outputs were affected by the change in temperature.

#### ***Staggered Interval Test***

This test was used to determine the effect of varying the lengths of the on periods. The testing consisted of a 5 minutes on interval, 10 minutes off, 15 minutes on interval, 10 minutes off, and 30 minutes on interval. Table 7 gives the test conditions.

Figure 11 shows the temperature profile for the staggered interval test. A similar pattern is seen in the 10-minute interval test, but now an asymptotic trend becomes clear during the 30-minute period. Figure 11 also includes an interval curve comparison showing that

**Table 6 High Vacuum Test Conditions for 10-Minute Interval Test**

Interval	Initial Pressure	Initial Temperature	Final Temperature
1	13.0 micro-Torr	40.6°C	56.7°C
2	11.2 micro-Torr	43.0°C	59.5°C
3	10.6 micro-Torr	43.4°C	60.0°C

**Table 7 High Vacuum Test Conditions for Staggered Interval Test**

Interval	Initial Pressure	Initial Temperature	Final Temperature
1	10.1 micro-Torr	42.4°C	55.3°C
2	9.78 micro-Torr	43.4°C	62.4°C
3	9.28 micro-Torr	45.0°C	64.0°C

the curves differ by less than two degrees at any point when overlapped. The y-axis accelerometer data indicates an asymptotic behavior as the temperature approaches a maximum.

#### ***Long Off Period Test***

The long off period test was run with intervals of 5 minutes on, 15 minutes off, 20 minutes on, 15 minutes off, and 5 minutes on. This test was used to compare with the short off-period tests. Figure 12 shows the trends and Table 8 gives the initial and final temperatures for this test.

**Table 8 High Vacuum Test Conditions for Long Off Period Test**

Interval	Initial Temperature	Final Temperature
1	36.3°C	50.6°C
2	37.8°C	60.5°C
3	39.4°C	52.5°C

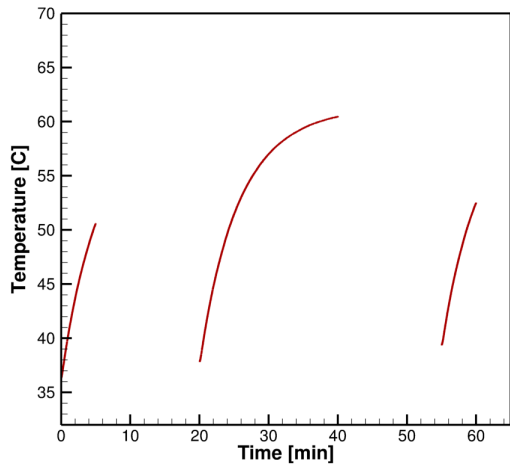


**Figure 12 Long Off Test At High Vacuum**

### IMU THERMAL MODEL

The measured IMU temperature histories can be used to extract thermal parameters such as the effective thermal mass of the device and its heat transfer coefficient at different environmental conditions. For the low Biot number conditions relevant to microelectronic devices, the temperature variation can be described by the simplified lumped capacitance approximation:

$$\frac{dT}{dt} = \frac{\dot{Q}}{mc_p} + \frac{hA}{mc_p}(T_a - T) \quad (5)$$

where  $c_p$  is the specific heat of the device,  $m$  is its mass,  $A$  is the area available for heat transfer, e.g. surface area of the device. Here  $T_a$  is the ambient temperature, which in this case is the initial temperature of the device in vacuum, and  $T_0$  is the initial device temperature. Here  $\dot{Q}$  is the heat generation rate, which is the fraction of input power to the device dissipated into heat. Figure 13 shows a sample heating and cooling curves for a process described by the model (5).

Assuming that the parameters in (5) do not vary significantly over the operating temperature range, an analytical solution for the device temperature is obtained as

$$T(t) = T_0 + \left( \frac{\dot{Q}}{hA} + (T_a - T_0) \right) \left[ 1 - \exp\left(\frac{-hA}{mc_p} t\right) \right] \quad (6)$$

From the measurements of temperature histories  $T(t)$  at different pressures and a known ambient temperature, one can use Eq. (6) to model the thermal performance of the IMU. For example, the steady-state temperature of the UM7-LT as shown in Figure 14 is  $T_\infty=58^\circ\text{C}$  for low ( $\sim 10\text{s mTorr}$ ) and  $T_\infty=64^\circ\text{C}$  for high-vacuum ( $\sim 0.01\text{ mTorr}$ ). From Equation (6):

$$T_\infty = \frac{\dot{Q}}{hA} + T_a \quad (7)$$

This allows (6) to be rewritten as

$$T(t) = T_0 + (T_\infty - T_0) \left[ 1 - \exp\left(\frac{-hA}{mc_p} t\right) \right] \quad (8)$$

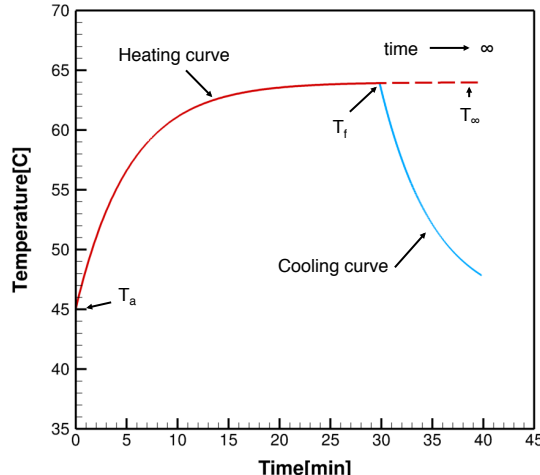


**Figure 13 Heating Curve Described by Equation 8; the Cooling Curve Is the Same Equation If Heat Dissipation Rate Is Assumed To Be 0**

From the data collected,  $T_\infty$  and  $T_a$  could be determined for given test conditions. This allows an exponential term to be approximated with a curve fit. A thermal model developed this way for low and high vacuum can be seen in comparison to the raw data in Figure 14. Table 9 includes the values of  $T_\infty$ ,  $T_a$ , and  $Ah/(mc_p)$  used for all three curves in Figure 14.

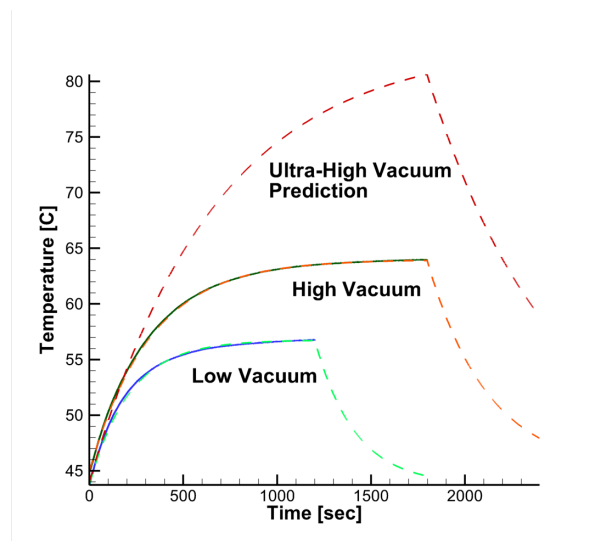


**Figure 14 Comparison of High Vacuum, Low Vacuum and Ultra-High Vacuum UM7-LT Temperatures. Solid lines – data, dashed – model**

The solid lines in the plots signify test data, while dashed lines represent the simulated output of the mathematical model.

**Table 9 Parameters for Low, High, and Ultra High Vacuum Thermal Models**

	$T_{\infty}$	$T_a$	$hA/(mc_p)$
<b>Low Vacuum</b>	56.8 °C	43.7 °C	-0.0047
<b>High Vacuum</b>	64.0 °C	45.0 °C	-0.0031
<b>Ultra-High Vacuum</b>	82.0 °C	44.0°C	-0.0015

It is useful to understand low and high-vacuum thermal behavior for the IMU for testing, but it is also important to know the behavior in ultra-high vacuum ( $10^{-9}$  Torr), where many small satellites operate in space.

The heat transfer coefficient will change for the device depending on the pressure during the test. During these experiments, the heat generation rate, specific heat and mass of the sensor were unknown and can be assumed constant. From the temperature data, we can determine the ratio of heat transfer coefficient at different pressures. For the data in Table 9, the heat transfer coefficient in high vacuum is 1.52 times lower than that in low vacuum. Assuming that for ultra-high vacuum the heat transfer coefficient reduces further by an additional factor of 2, the steady-state temperature at ultra-high vacuum of the UM7-LT would be 82 °C and  $hA/(mc_p)=-0.0015$ . These parameters allow a prediction curve to create a duty cycle for operation in ultrahigh vacuum to be generated as in Figure 15.

From these parameters it is easy to see a need for a duty cycle to prevent damage to or failure of the IMU. Figure 15 shows a duty cycle that was developed for the high vacuum thermal model. The on cycles are 20 minutes and the off cycles are 20 minutes. The off cycles were chosen as it takes 17.5 minutes to return to within 2% of the ambient temperature.

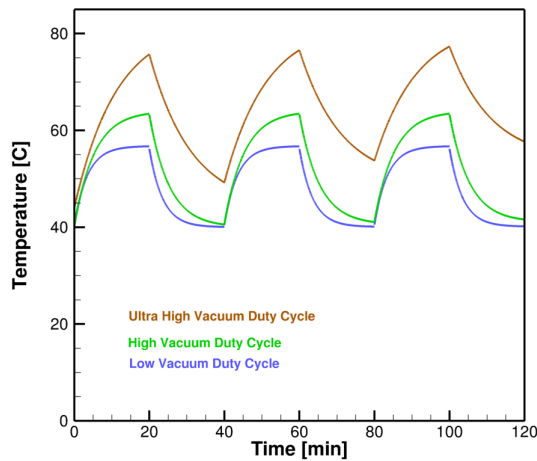


**Figure 15 IMU Duty Cycle for Low, High, and Ultra-High Vacuum**

## RASPBERRY PI ZERO TEMPERATURE TESTS

The Raspberry Pi Zero W serves as the experimental general-purpose computer. In the context of this research they are used for data collection inside the vacuum chambers and as a stand in for a bus on a CubeSat. With a small form factor and interfaces common for sensors and other electronics, the Raspberry Pi enables far faster development time than any specialized control system permits. This is valuable when developing technologies or testing payloads, where the primary focus is on developing a subsystem rather than preparing a satellite for space. Running a true operating system, the device can be programmed for a number of functions necessary for both controlling a satellite or subsystem and evaluating its performance. In particular, experimental data is collected from the various sensors and written to the Raspberry Pi's onboard Secure Digital (SD) card for later analysis.

Despite its utility for developing and testing CubeSat related technologies and subsystems, the Raspberry Pi is not intended for use in a flight-ready satellite. In addition to not being rated for space, the Raspberry Pi is not ideal for flight for a few reasons. Although running an operating system significantly lowers development time, the presence of background

processes introduces novel issues specialized hardware do not face.

First, background processes often consume energy to perform computations not needed during an experiment. This not only uses CPU cycles, but also increases the energy consumption of the system, which currently sits at half a Watt during normal operation. To mitigate this effect, unnecessary software has been removed from the system, most notably the graphical interface and programs that attempt to access the internet.

Furthermore, the Raspberry Pi's single-core CPU permits only one process to execute instructions at a time. Therefore, the Linux Kernel uses a complex and nondeterministic scheduling system for deciding when processes run and for how long. This means that whenever something besides the experimental software is selected for execution, all measurements, logging, GPIO control changes, and other aspects of the experimental software's operation have to be put on hold. Although changing system priority can alleviate some of these preemptions, it is a necessary feature of the vanilla Linux Kernel. Using a real-time patch to the Linux Kernel may eliminate this issue.

#### **Thermal Testing in Low Vacuum**

To better understand the thermal properties of the Raspberry Pi Zero's Central Processing Unit (CPU) before use in the metallic vacuum chamber, we prepared a smaller, small vacuum chamber to stress test the computer.

The Raspberry Pi running at minimal load was placed into the vacuum chamber and allowed to equilibrate as the air was pumped out of the chamber until a pressure of 55 milli-Torr was observed. After reaching equilibrium for 77 seconds, the CPU executed at maximal load for 22.75 minutes during which the temperature climbed and eventually plateaued. Then the CPU returned to minimal load, causing the temperature to sharply drop and approach the initial equilibrium.

As an experimental control, the same procedures were followed but with the pressure at a constant 1 atm. Similar in form but different in scale, the curves formed in the comparison plot in Figure 16 indicate key thermal properties of the CPU. The comparison of the atmospheric and the low vacuum tests are shown in Figure 16. Most notably, heat transfer from convection to the air allowed the CPU under 1 atm. to reach a peak temperature of only 44.4°C, almost 20 degrees less than that achieved by device in the low vacuum (62.3°C).

Although the observed 62.3°C is within the Raspberry Pi's recommended 70°C operating limit, the small vacuum chamber was not a representative of expected high-vacuum usage conditions.

#### **Raspberry Pi Zero Thermal Model**

Using the collected data from testing in air (at 1 Atm) and in low vacuum,  $T_\infty$  and  $T_a$  could be determined. Using curve fitting, the exponential term was approximated, and a model was developed for the Raspberry Pi Zero for air, low vacuum and high vacuum. The comparison can be seen in Figure 16. Table 10 includes the values of  $T_\infty$ ,  $T_a$ , and  $Ah/(mc_p)$  used for all three curves.

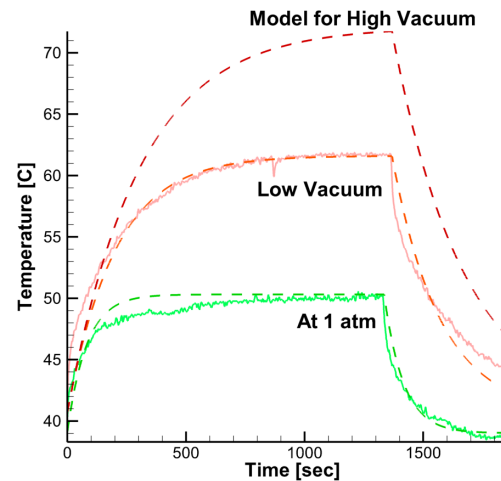


**Figure 16 Comparison of High Vacuum, Low Vacuum and In-air Thermal Data and Models for Raspberry Pi Zero**

The solid lines in the plots signify test data, while dashed lines represent the simulated output of the mathematical model.

**Table 10 Parameters for In-Air, Low and High Vacuum Thermal Models**

	$T_\infty$	$T_a$	$hA/(mc_p)$
<b>At 1 atm</b>	50.3 °C	39.0 °C	-0.0123
<b>Low Vacuum</b>	61.6 °C	40.6 °C	-0.0049
<b>High Vacuum</b>	72.1 °C	40.6 °C	-0.0033

The high vacuum thermal model is based on the assumption that the heat transfer coefficient varies by a factor of 0.67 from low to high vacuum, as was the observed case for the UM7-LT. Additionally, it is assumed that the heat generation rate, specific heat, and mass of the device remain constant under different pressure conditions.

### Thermal Testing in High Vacuum

Thermal tests in the large vacuum chamber were performed on board the 1U-FEMTA CubeSat Model, which is used to test the Film-Evaporation MEMS Tunable Array (FEMTA) micropropulsion system. During the test, the CubeSat model radiatively dissipates heat. Since the Raspberry Pi is not designed to perform in such an extreme thermal environment, the CPU was monitored using the on-board thermometer.

The CPU was running at 25-30% of the maximum load during the large chamber test. The maximum temperature measured during the test was 58.4°C. The Temperature profile is shown in Figure 17. The Raspberry Pi Zero has a lower maximum temperature during this test but this can be primarily accounted for in the reduction in load.

In one instance, during a separate test with the Raspberry Pi in the large vacuum chamber, the CPU thermometer read values up to 99.8°C, putting the boiling point of water within the margin of error. This occurred despite the load maintaining a consistent 20-30% utilization rate. This difference may be accountable from the difference in emissivity of the acrylic versus the metallic walls of the chamber. To a lesser extent, the packing of modules in the CubeSat may have lowered the device's ability to radiate, as the CPU was perfectly exposed in the small chamber.

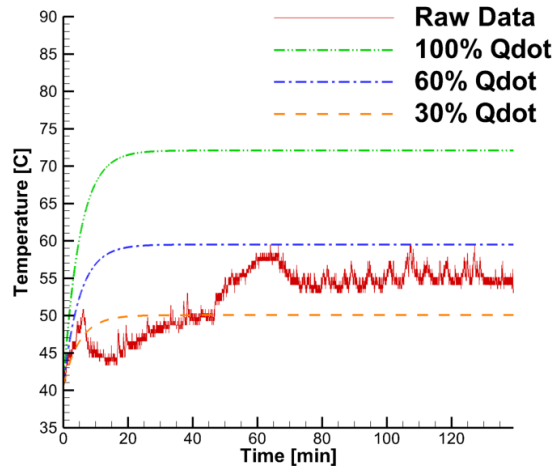


**Figure 17 High Vacuum Chamber Thermal Test of Raspberry Pi Zero**

For the first 45 minutes of operation, the CPU was running at 25-30% of the maximum load. After this point, CPU usage went up to 50-60%. As seen in Figure 17, the thermal profile fits the prediction of the analytical model, given the assumption that the heat generation rate varies from the maximum value, at the

same factor as CPU usage, i.e. for 30% CPU usage,  $\dot{Q}' = 0.30 * \dot{Q}$ .

### CONCLUSIONS

The objective of this research was to quantify the thermal behavior of the UM7-LT COTS IMU in low and high vacuum environments. COTS sensors, such as IMUs, are valuable tools for testing small satellite technology and subsystems.

Initial testing was done with thermal imaging to determine which of the IMU components generated the most heat, revealing that the Processing IC produces the bulk of the heat on the device. Tests were then conducted in low and high vacuum. The gyroscope, accelerometer, and magnetometer all showed signs of thermal drift due to the temperature increase of the IMU in both low and high vacuum. This drift can be fitted with a second order polynomial to correct the output and remove the thermal drift. Given the data collected, it is possible to create an analytical model based on lumped capacitance heat transfer analysis to predict a functional duty cycle for the device to help mitigate the effects of thermal drift. Similar analysis can be applied to assembly-level thermal testing.

### References

- Heidt, H. et. al., "CubeSat: A new Generation of Picosatellite for Education and Industry Low-Cost Space Experimentation," Proceedings of the 14<sup>th</sup> AIAA/USU Conference on Small Satellites, Logan, Utah, August 2000.
- Toorian, A. et. al., "CubeSats as Responsive Satellites," Long Beach, California, August 2005
- Bok, C. et. al., "SmallSats by the Numbers 2018," Bryce Space and Technology, Alexandria, Virginia, 2018.
- "Achieving Science with CubeSats: Thinking Inside the Box", The National Academies Press, Washington, D.C., 2016.
- Woellert, K., et al., "CubeSats: Cost-effective science and technology platforms for emerging and developing nations," Advances in Space Research, vol. 47, issue 4, February 2011.
- Goggin, M. et. al., "CubeSat Sensor Platform for Reentry Aerothermodynamics," Proceedings of the 31<sup>st</sup> AIAA/USU Conference on Small Satellites, Logan, Utah, August 2017.
- Swartz, W. et. al., "RAVAN CubeSat Results: Technologies and Science Demonstrated on Orbit," Proceedings of the 31<sup>st</sup> AIAA/USU Conference on Small Satellites, Logan, Utah, August 2017.

8. Williams, C., Doncaster, B., Shulman, J., "2018 Nano/Microsatellite Market Forecast," SpaceWorks, Atlanta, Georgia, 2018.
9. Peck, M., et al., "NASA Strategic Space Technology Investment Plan," 2012.
10. Spann, J., "NASA Perspectives on CubeSat Technology and Highlighted Activities," SNAP Nanosatellite/CubeSat Subject Matter Expert Exchange, Brasilia, Brazil, June 2016.
11. Morrison, M., "Inertial measurement unit," U.S. Patent No. 4,711,125, December 1987.
12. Dussy, S., "MEMS gyro for space Application," Proceedings of the AIAA Guidance, Navigation, and Control Conference, San Francisco, California, August 2005
13. Wyatt, C.L., *Radiometric Calibration: theory and methods*. Elsevier, 2012.
14. "Low Profile Six Degree of Freedom Inertial Sensor: ADIS 16334," Analog Devices, Inc. Norwood, Massachusetts, 2011.
15. Blackwell, W., et al., "MicroMAS: A First Step Toward a Nanosatellite Constellation for Global Storm Observation," Proceedings of the 27<sup>th</sup> AIAA/USU Conference on Small Satellites, Logan, Utah, August 2013.
16. "High Precision Tri-Axis Inertial Sensor: ADIS16350/ADIS16355," Analog Devices, Inc. Norwood, Massachusetts, 2007.
17. MoonJelly, P. et al., "Development of a Low-Cost, Low-Power Attitude Determination System for a Nano-Satellite," Proceedings of the AIAA/AAS Astrodynamics Specialist Conference and Exhibit, Honolulu, HI, 2008.
18. "Triaxial Inertial Sensor with Magnetometer: ADIS16405," Analog Devices, Inc. Norwood, Massachusetts, 2009.
19. Shiotani, B., et al., "Reliability Analysis and Risk Management of SwampSat Space Systems Group," Proceedings of The 5<sup>th</sup> Nano-Satellite Symposium, Tokyo, November 2013.
20. "Six Degrees of Freedom Inertial Sensor: ADIS16360/ADIS16365," Analog Devices, Inc. Norwood, Massachusetts, 2009.
21. Okseniuk, K., "Prox-1: Automated Proximity Operations on an ESPA Class Platform," Proceedings of the 29<sup>th</sup> AIAA/USU Conference on Small Satellites, Logan, Utah, August 2015.
22. "Tactical Grade, Six Degrees of Freedom Inertial Sensor: ADIS16485," Analog Devices, Inc. Norwood, Massachusetts, 2012.
23. Jeremie, M., "Characterization of atmospheric signals seen by a 350km CubeSat," ISAE SUPAERO, June 2014.
24. "Epson Europe Electronics GmbH M-G364PDCA," Epson Europe Electronics GmbH. Munich, <https://geo-matching.com/category/inertial-measurement-units-imus/m-g364pdca>
25. Jehle, A., "Iodine Small Satellite Propulsion Demonstration iSAT," Proceedings of the 31<sup>st</sup> AIAA/USU Conference on Small Satellites, Logan, Utah, August 2017.
26. "UM7 DATASHEET," CH Robotics, Box Hill North, Victoria, Australia, January 2016.
27. "VectorNav Industrial Series," VectorNav Technologies, Dallas, Texas, 2017.
28. Janson, S., "The NASA Optical Communication and Sensor Demonstration Program: An Update AeroCube-OCSD mission," Aerospace Corporation, August 2014.
29. "MPU-6000 and MPU-6050 Product Specification," InvenSense Inc., Sunnyvale, California, 2013.
30. Mačiulis, L., "LituanicaSAT-2: Design of The 3U In-Orbit Technology Demonstration CubeSat," IEEE Aerospace and Electronic Systems Magazine, vol. 32, issue 6, June 2017.
31. "Lord Datasheet: 3DM-GX5 Inertial Measurement Unit (IMU)," Lord Corporation, Williston, Vermont, 2018
32. Bandon, C., "Lessons Learned on a Successful CubeSat Launch," Proceedings of the 11<sup>th</sup> Annual CubeSat Developers Workshop, San Luis Obispo, California, 2014.
33. Fried, L., "Introducing the Raspberry Pi Zero," Adafruit Industries, New York City, New York, 2017.